Altered synaptic ultrastructure in the prefrontal cortex of Shank3-deficient rats

Sarah Jacot-Descombes
University Hospital and School of Medicine, Geneva
Neha U Keshav
Icahn School of Medicine at Mount Sinai
Dara L. Dickstein
Uniformed Services University of the Health Sciences
Bridget Wicinski
Icahn School of Medicine at Mount Sinai
William G. M. Janssen
Icahn School of Medicine at Mount Sinai
Liam Hiester
Icahn School of Medicine at Mount Sinai
Hala Harony-Nicolas
Icahn School of Medicine at Mount Sinai
Joseph D. Buxbaum
Icahn School of Medicine at Mount Sinai
Patrick R. Hof
Icahn School of Medicine at Mount Sinai
Merina Varghese (✉ merina.varghese@mssm.edu)
https://orcid.org/0000-0002-1517-3903

Research

Keywords: autism spectrum disorder, Phelan-McDermid syndrome, synapse morphology, electron microscopy

Posted Date: January 13th, 2020

DOI: https://doi.org/10.21203/rs.2.20698/v1

Version of Record: A version of this preprint was published on November 17th, 2020. See the published version at https://doi.org/10.1186/s13229-020-00393-8.

Abstract

Background

Deletion or mutations of SHANK3 lead to Phelan-McDermid syndrome and monogenic forms of autism spectrum disorder. SHANK3 encodes its eponymous scaffolding protein at excitatory glutamatergic synapses. Altered dendritic and spine morphology in the hippocampus, cerebellum and striatum have been associated with behavioral impairments in various Shank3-deficient animal models. Given the attentional deficit reported in these animals, our study explored whether deficiency of Shank3 in a rat model alters synaptic ultrastructure in the medial prefrontal cortex.

Methods

We used electron microscopy to determine the density of asymmetric synapses in layer III excitatory neurons of the medial prefrontal cortex in 5 week-old Shank3-homozygous knockout (Shank3 -KO), heterozygous (Shank3 -Het), and wild-type (WT) rats. We also measured postsynaptic density length, postsynaptic density area, and head diameter of dendritic spines at these synapses.

Results

All three groups had comparable synapse density and postsynaptic density length. Spine head diameter of Shank3 -Het rats, but not Shank3 -KO, was larger than WT rats. Shank3 -Het rats had wider head diameter in non-perforated synapses compared to WT and Shank3 -KO rats. The total postsynaptic density area was significantly larger in Shank3 -Het rats compared to Shank3 -KO and WT rats. These findings represent preliminary evidence for synaptic ultrastructural alterations in the medial prefrontal cortex of rats that lack one copy of Shank3 and mimic the heterozygous loss of SHANK3 in Phelan-McDermid syndrome.

Limitations

The Shank3 deletion in the rat model we used does not affect all isoforms of the protein and as such, would only model the effect of the mutations resulting in loss of the N-terminus of the protein. Given the higher prevalence of ASD in males, this study focused only on synaptic ultrastructure in male Shank3 -deficient rats.

Conclusions

We observed increased head diameter and postsynaptic density area in rats heterozygous for Shank3 deficiency. Further investigations of the mechanisms leading to altered synaptic ultrastructure in this animal model will enable us to understand better the role that Shank3 protein plays in autism spectrum disorder and Phelan-McDermid syndrome.

Background:

Autism spectrum disorder (ASD) is a neurodevelopmental disorder affecting 1 in 59 children in the United States (1). Individuals diagnosed with ASD show difficulty in social interaction and communication and restrictive, repetitive behaviors from an early age (2). ASD is a common comorbid condition in individuals with Fragile X syndrome, Rett syndrome, Phelan-McDermid syndrome (PMS), and other genetic disorders (3). Studying the cellular mechanisms affected by the genes identified in these monogenic disorders has helped to understand the pathophysiology underlying ASD better (reviewed in (4)).

Deletions in chromosome 22q13, which encompasses several genes including SHANK3, cause PMS (also known as deletion 22q13.3 syndrome) (5, 6). Deletion and point mutations of SHANK3 also cause PMS (7–9) and haploinsufficiency of SHANK3 is linked to many of the neurological symptoms in subjects with PMS (7, 9–12). Children with PMS show global developmental delay, delayed or absent speech, moderate to severe intellectual disability, hypotonia, seizures, and psychiatric features including ASD, attention-deficit/hyperactivity disorder (ADHD) and bipolar disorder (6, 7, 13–16). Mutations of SHANK3 have also been identified as a major monogenic cause of ASD (17, 18).

SHANK3 encodes the SH3 and multiple ankyrin repeat domains protein 3 that belongs to a family of proteins also including Shank1 and Shank2. The Shank proteins interact with multiple other proteins, including cell adhesion proteins at the synapse, cytoskeletal proteins within the dendritic spine and, via other scaffolding proteins, with ionotropic and metabotropic glutamate receptors (mGluRs) at the postsynaptic density (PSD) of excitatory synapses (19–22). Starting from the N-terminus to the C-terminus, the Shank proteins share five protein-protein interaction domains: a multiple ankyrin repeats domain (ANK), an SRC homology domain 3 (SH3), a PSD-95/Disc Large homolog-1/Zonula occludens-1 domain (PDZ), a proline-rich cluster domain (PRC) and a sterile alpha-motif domain (SAM) (23). All three Shank family members share domain structures that are 60–90% similar except for the PRC domain (33–40%) (21). Guanylate kinase-associated protein (GKAP) bound at the PDZ domain and Homer bound at the PRC domain of Shank proteins enable recruitment of ionotropic N-methyl-D-aspartate (NMDA) receptors and mGluRs respectively to the PSD (20, 24). Shank3 also directly interacts with subunits of ionotropic amino-3-hydroxy-5-methylisoxazole-4-propionic acid (AMPA) receptors at its PDZ domain (25, 26). Shank proteins interact with PSD scaffolding proteins and cytoskeletal actin mediated through cortactin binding at their PRC domains, to regulate the structure of dendritic spines (27). Thus, all three Shank proteins have roles in assembling and stabilizing PSD complexes and regulation of spine structure, driven by activity at the synapse (20, 28, 29) and their altered expression may contribute to the behavioral deficits in ASD and PMS.

Individuals with ASD have deficits in social communication and restricted, repetitive or unusual sensory-motor behaviors. A possible reason for the deficits in social communication and interaction shown by subjects with ASD is their difficulty understanding the emotional behavior of others (1, 2). The prefrontal cortex (PFC) is known for its role in cognitive control, coordinating memory, planning and executive activity (30, 31). The orbitofrontal cortex in the PFC is also a major part of the network that processes empathy and social behavior (32). Structural and functional abnormalities in the PFC have been demonstrated in patients affected by ASD (33–38). As 80% of PMS patients present with ASD, the PFC

could be similarly altered in PMS. Moreover, other psychiatric features seen in PMS (6, 13), such as attentional deficit (39, 40), anxiety (41), bipolar disorder (42), and schizophrenia (43, 44) as well as comorbidities in ASD, such as ADHD, intellectual disability, anxiety, irritability and aggression, epilepsy and sleep disturbances (45, 46), also implicate the PFC.

Here, we use a Shank3-deficient rat model to investigate potential synaptic changes in the PFC caused by mutations in Shank3. The infralimbic and prelimbic cortex in the rat are generally considered to be homologous in function to the medial PFC (mPFC) in humans (47), as these regions in the rat are required for working memory tasks, attentional tasks, emotional regulation, behavioral flexibility and forms of associative learning (48–52). Given the prominent role of Shank3 at the PSD (53, 54), as well as the synaptic plasticity deficits in the mPFC and the attentional deficit seen in this Shank3-deficient rat model (55), we hypothesized that loss of Shank3 would affect synapse density and ultrastructure of dendritic spines in the PFC of Shank3-deficient rats.

Methods

Animals

We used the Shank3-deficient rat model created by zinc-finger nuclease technology. This rat model harbors a deletion of 68 base pairs in exon 6 of the ANK domain, generating a stop codon that truncates expression of the full-length Shank3 protein (55). A similar truncation was observed in a patient with PMS who carried a c.601–1G > A mutation in SHANK3 (56). The resulting reduction of Shank3 expression in rats causes deficits in social recognition memory and attention (55). Here, we used male rats (n = 18) at 5 weeks of age from three groups, wild-type (WT), Shank3 heterozygote (Shank3-Het) and Shank3 knockout (Shank3-KO). Our study followed the National Institute of Health Guidelines for the Care and Use of Experimental Animals and all animal protocols were approved by the Institutional Animal Care and Use Committee at the Icahn School of Medicine at Mount Sinai.

Perfusion and tissue processing

Rats were anesthetized using 30% chloral hydrate and intracardially perfused with 1% paraformaldehyde (PFA) in phosphate buffer (PB, pH 7.4) for 2 min, followed by a fixative comprising 4% PFA and 0.125% glutaraldehyde in PB for 10 min. The brains were immediately dissected, post-fixed overnight at 4°C in 4% PFA and 0.125% glutaraldehyde in PB, and then transferred to phosphate buffered saline with 0.1% sodium azide at 4°C until sectioned. The brains were hemisected and the right hemisphere was cut into 250 ∝m-thick sections using a vibratome (VT1000S, Leica Microsystems, Buffalo Grove, IL). The sections were cryoprotected in a graded glycerol/PB solution after which the mPFC was microdissected into blocks that underwent cryosubstitution and low-temperature embedding as described earlier (57). Five consecutive ultrathin sections were cut at 90 nm using a diamond knife (Diatome, Hatfield, PA) on an ultramicrotome (Reichert-Jung, Depew, NY) and mounted onto a Formvar-supported slot grid (Electron Microscopy Sciences, Hatfield, PA).

Morphological analysis

Serial sections from each animal were imaged at 75 kV on an H-7000 transmission electron microscope (Hitachi High Technologies America, Clarksburg, MD) with an AMT Advantage CCD camera (Advanced Microscopy Techniques, Woburn, MA). Fourteen to 17 sets of images were collected from layers II and III in the mPFC in the five serial sections at a magnification of 17,000. Electron micrographs were adjusted for brightness, contrast, and sharpness and morphological analysis was carried out using Photoshop CS5 (version 12.0, Adobe, San Jose, CA).

Axospinous synapses were identified by their asymmetric PSD, a clear synaptic cleft and the presence of vesicles in the presynaptic axonal bouton. Synapses were analyzed by the disector method (58), as described in our previous studies (57, 59). Briefly, we identified synapses across two pairs of layers, the reference layer (sections one and five) and the lookup layer (sections two and four), from five serial sections and counted only the unique synapses found either in the reference layer or in the lookup layer (Fig. 1). Perforated synapses were identified by the presence of a clear gap in the middle of the PSD, in any of the layers where the PSD was visible starting from the unique synapse in the second layer (Fig. 1,2). We subtracted the number of perforated synapses from that of the total synapses to obtain the number of non-perforated synapses. The disector area was 42.77 μm^2, and disector height was 0.18 μm; therefore, synapse density was calculated as the total number of counted synapses of each type (perforated, non-perforated and total) from both the first and second pair of layers divided by the total volume of the disector (7.70 μm^3). An average of 12.08 unique synapses were counted from each animal.

The length of the PSD and the maximal head diameter (HD) were measured starting with the unique PSDs identified in the first set of lookup layers (Sect. 2 and 4) and proceeding through the series either forward (from Sect. 2) or in reverse (from Sect. 4) (Fig. 2). For the measurement of the PSD length in non-perforated synapses, we measured the maximal length of the PSD (Fig. 2A). For perforated synapses, we added each length of the different segments of the PSD to obtain the maximal PSD length (Fig. 2B). The HD was measured using the maximal length of the spine head parallel to the PSD (Fig. 2). The PSD length and the HD were measured in all the four layers if they were visible (Fig. 2). For the HD, the largest HD among all four layers was represented as the maximal HD of the synapse (Fig. 2). Similarly, for the PSD length, only the longest PSD length was used. However, the PSD area was calculated by multiplying the PSD length with the thickness of the layer (0.09 μm) and adding together the results for each layer. The measurements of PSD length and head diameter were obtained at a resolution of 0.5 μm/137 pixels.

Statistical analysis:

Comparisons of potential genotypic variations were determined using one-way analysis of variance (ANOVA) corrected for multiple comparisons using the Tukey's post hoc test. Calculations were performed using GraphPad Prism (version 5.01, GraphPad Software, San Diego, CA). Statistical significance was set at an α level of 0.05

Results:

Synapse density was unchanged in Shank3-deficient rats compared to controls

We did not find any differences in total synapse density in Shank3-Het or Shank3-KO rats compared to WT controls ($F_{[2,15]} = 2.91$, $p = 0.09$, Fig. 3A-D). Non-perforated (Fig. 3E) and perforated synapse densities (Fig. 3F) were also comparable ($F_{[2,15]} = 3.27$, $p = 0.07$ and $F_{[2,15]} = 0.34$, $p = 0.72$, respectively) in Shank3-Het or Shank3-KO rats and controls.

Subtle changes in synaptic ultrastructure were present in Shank3 heterozygotes

We did not find any differences in total PSD length when comparing Shank3-Het or Shank3-KO rats to the WT group ($F_{[2,15]} = 2.90$, $p = 0.09$; Fig. 4A). Additionally, the PSD lengths of non-perforated ($F_{[2,15]} = 2.60$, $p = 0.11$, Fig. 4B) and perforated synapses ($F_{[2,15]} = 1.99$, $p = 0.17$; Fig. 4C) were comparable between Shank3-deficient and WT rats.

However, PSD area and maximal HD were altered in the Shank3-Het group, but not in the Shank3-KO, when compared to the WT. Total HD was significantly higher ($F_{[2,15]} = 4.03$, $p = 0.04$) in the Shank3-Het rats as compared to the WT (Fig. 4D). We also found wider ($F_{[2,15]} = 5.48$, $p = 0.02$) HD of non-perforated synapses in the Shank3-Het group compared to both WT and Shank3-KO rats (Fig. 4E). When we analyzed only the perforated synapses, there was no significant change in HD among the groups ($F_{[2,15]} = 1.18$, $p = 0.34$; Fig. 4F).

The total PSD area was greater ($F_{[2,15]} = 5.14$, $p = 0.02$) in the Shank3-Het rats compared to both the other groups, WT and Shank3-KO (Fig. 4G). There was no significant change in PSD area among the three groups, WT, Shank3-Het and Shank3-KO when we divided the synapses into non-perforated ($F_{[2,15]} = 3.30$, $p = 0.07$; Fig. 4H) and perforated ($F_{[2,15]} = 1.08$, $p = 0.37$; Fig. 4I).

Discussion

The interaction of Shank proteins with their various partners can be regulated by several mechanisms. First, alternative exon splicing results in multiple splice variants of Shank3 in the human brain (17). Splice sites are present downstream of the SH3 and PDZ domains and within the PRC and SAM domains of Shank3 (25) and the human brain shows higher expression of exons encoding these functional regions (60). Second, Shank3 has six intragenic promoters resulting in differential expression of isoforms, named Shank3a through Shank3f, during brain development (25, 61, 62). Finally, the subcellular and tissue-

specific patterns of expression and turnover of Shank isoforms during development and synaptic activity are also regulated by methylation (63–65) and ubiquitination (66).

The Shank3 rat model used here demonstrated attentional deficit and reduced hippocampus-to-mPFC signaling in both Shank3-Het and Shank3-KO rats compared to WT (55), pointing towards a synaptic deficit in the mPFC. The synaptic deficits may be due to either changes in synapse density or decreased recruitment of proteins to the PSD that would be visible as ultrastructural changes of the PSD or spine head. Our results show no significant change in the total density of excitatory synapses among the three experimental groups at 5 weeks of age. Although few studies have assessed synapse density per se, our results are corroborated by previous reports showing no change in spine density in the neocortex of Shank3-Het mice (67) and in the hippocampus of Shank3-KO mice with an exon 21 deletion (68). However, other studies have reported a significant decrease in spine density in Shank3-deficient models compared to controls, as observed in neurons differentiated from human induced pluripotent stem cells carrying SHANK3 mutations (69), the PFC of a macaque model with deletions in exons 6 and 12 (70), the hippocampus of 5-week-old Shank3-KO rats with deletion of exons 11–21 and loss of all the Shank3 isoforms (71), the striatum of 5-week-old Shank3-KO mice lacking Shank3b following deletion of exons 13–16 containing the PDZ domain (72), and the cerebellum of Shank3-Het mice with an exon 21 deletion (73). However, Shank3-KO mice with an exon 4–9 deletion and loss of the Shank3a and Shank3b isoforms bearing the ANK and SH3 domains showed decreased spine density in the hippocampus at 4 weeks of age, but no change at 10 weeks (74). Shank3-KO mice with exons 4–22 deleted and a complete loss of all Shank3 isoforms and splice variants showed decreased spine density only in the striatum, but not the hippocampus, at 8 weeks of age (75). In vitro studies have shown that full-length Shank3 was localized in dendritic spines, whereas a C-terminal truncated isoform was diffusely distributed in dendrites and axons (61) and the isoform length determined its effects on dendritic spine density (62). Thus, the age of the animal, the extent of Shank3 deletion, and the brain regions examined, all determined whether synaptic density was altered in Shank3-deficient animals.

Synapses show different structures, with perforated or non-perforated PSDs according to changing neurotransmission efficacy in response to activity (76, 77) and function (76–79). We did not observe any differences in density of non-perforated or perforated synapses in the PFC among the three genotypes of rats. However, in the hippocampus of 5-week old Shank3-Het mice where the ANK domain was deleted, non-perforated synapse density was unchanged but perforated synapse density was higher as compared to the Shank3-KO and WT groups; this change was not present at 3 months of age (59). The observed difference in density of the perforated synapses between the two Shank3 models may be due to different effects of Shank3 in the two brain areas studied.

Maximal PSD length was unchanged, but PSD area and HD were increased in the Shank3-Het group and not in the Shank3-KO as compared to WT rats. The PSD area was calculated using the PSD length across the series of sections where the synapse was visible. We did not find a significant increase in maximal PSD length, leading us to suppose that the observed change in PSD area is small but significant when adding the PSD length across the thickness of the dendritic head to find the PSD area. The observed

change in size of the spine head could also modify the PSD area. Similar to our results, PSD length and thickness were unchanged in hippocampal CA1 neurons of Shank3-KO mice with an exon 4–9 deletion (74). In a different model with a similar deletion, PSD length and area as well as HD were unchanged in the hippocampus of both Shank3-Het and Shank3-KO mice compared to WT at 5 weeks and 3 months of age (59). These results were confirmed in the hippocampus of Shank3-KO mice with exon 4–21 deletion, but in the striatum of these mice, decreased PSD length and thickness were seen at 8 weeks of age (75). Of note, the increase in PSD area and HD that we observed was present only in the Shank3-Het rats compared to WT and no change in the synaptic ultrastructure was observed in the Shank3-KO group. The Shank3-Het rats carry one copy of undeleted Shank3 that can express the full-length isoforms of the protein, though at lower levels than the WT. Shank3-KO rats express no full-length Shank3 and the truncated isoforms in these animals may not be sufficient to recruit the Shank3 binding partners in the PSD that potentially compensate for this lack in the Shank3-Het rats. The Shank3-KO rats may be able to maintain the structure of dendritic spines and the PSD comparable to WT through the shorter Shank3 isoforms or by recruiting the other Shanks to the PSD. Although the ANK domain of Shank3 is deleted in our model, the synapse-targeting SAM domain as well as the major binding sites on Shank3 for recruiting the NMDA and AMPA receptors to the PSD and for binding cytoskeletal proteins essential for spine morphology are preserved in the Shank3-KO and may be sufficient to maintain synaptic morphology at a level similar to that in the WT.

In the Shank3-Het rats that carry only one copy of the gene and can express full-length Shank3 together with the shorter isoforms, the other Shank family proteins may compensate for the loss of Shank3, resulting in the observed increase in size of the dendritic head and PSD area. Shank2, that shares both a homologous PRC domain and a synapse-targeting C-terminal region with Shank3 (22, 28), seems to be the better candidate to compensate for reduced Shank3 expression. Indeed, Shank2 with an intact PRC domain can rescue reduced head diameter of dendritic spines in hippocampal neurons, induced by a knockdown of all three Shank proteins (80). Overexpression of Shank1 containing the PRC domain also results in enlargement of spine head size (81). In contrast to our results, decreased spine head volume was observed in human neurons differentiated from induced pluripotent stem cells sourced from subjects with Shank3 mutations (69). Furthermore, a deletion of the ANK-SH3 domains of Shank3 results in reduced spine head area in mouse hippocampal neurons (53). In our Shank3-Het rat model, not only are low levels of the full-length Shank3 protein expressed, but also shorter isoforms lacking the ANK domain but containing the PDZ domain which recruits NMDA and AMPA receptors during spine maturation (53), the PRC domain where Homer1 and cortactin bind (20, 21, 25), and the synapse-targeting SAM domain (61). Thus, overcompensation by the full-length protein recruiting the shorter Shank3 isoforms or other Shank proteins and giving an enlargement of the HD and PSD area seems probable.

PSD fractions from the neocortex of Shank3-Het and Shank3-KO rats with exons 11–21 deleted in Shank3 (71) and hippocampal neurons after knockdown of four major isoforms of Shank3 in vitro show no change in Shank1 or 2 expression (82), but other compensatory mechanisms may occur in vivo in the PFC. A study in the mouse brain found that proteins interacting with Shank3 in the PFC are different from those in the hippocampus and striatum (83). Dimethylation of histone lysine 9 following higher

expression of euchromatic histone methyltransferases is found in the PFC, but not striatum or hippocampus, of 5- to 6-week-old Shank3-Het mice with an exon 21 deletion and also in BA9 from postmortem ASD brains, suggesting a brain region-specific mechanism for regulation of protein expression (84). The same mouse model also shows low levels of histone acetylation in the PFC as compared to WT mice (85). Notably, the expression of Shank3 is highest in the PFC compared to other regions in the macaque brain (70), whereas Shank3 isoforms containing ANK domain are highly expressed in the upper cortical layers, hippocampus and striatum of the mouse brain (86). Multimer formation of Shank proteins may enable their recruitment to the synapse without an overall increase in protein concentration. Shank1 forms multimers via interactions between ANK repeats and SH3 domain (87) or PDZ domains (88). The same is true of Shank3 via its PRC and SAM domains (20), although these interactions remain to be proven endogenously in neurons. Interestingly, the interaction of ANK repeats and SH3 domains in Shank1 is reported to require all the repeats in the ANK domain (87) and, if this extends to Shank3, the lack of the ANK domain in Shank3 of the Shank3-KO rats could explain their difference from the Shank3-Het rats in our study. Despite these potential compensatory mechanisms for some functions when Shank3 is deficient, the presence of clinical phenotypes due to Shank3 haploinsufficiency in humans carrying SHANK3 mutations (6, 7, 9, 13) and of behavioral deficits in animal models with Shank3 deficiency (55, 67, 71, 89) suggests such compensation may not be fully effective to rescue the functional phenotype but may be able to partially preserve the ultrastructure of synapses.

Limitations:

Although the prevalence of PMS is equal in both sexes (90), ASD occurs four times more frequently in males than females (1). This study used only male mice to uncover synaptic changes in the PFC relevant to both ASD and PMS. The deletion in exon 6 of the Shank3 gene would affect the N-terminal ANK domain, truncating the full-length protein, but shorter isoforms of Shank3 may still be expressed in the Shank3-Het and Shank3-KO rats. Thus, the changes observed using this rat model would more accurately reflect the effects of mutations affecting the N-terminal of the protein than those resulting from deletion of the gene and the loss of all isoforms of the protein.

Conclusions:

The increase in PSD area and size of the spine head in the Shank3-Het rats, but not the Shank3-KO, may more accurately model synaptic changes occurring from haploinsufficiency of SHANK3 that is linked to the neurological symptoms in PMS. These changes in the PFC at the level of synaptic ultrastructure may have implications for the attentional deficit observed in Shank3-Het rats, and also in subjects with PMS and ASD who carry mutations in SHANK3.

Abbreviations

PMS
Phelan-McDermid syndrome
ASD
autism spectrum disorder
SHANK3
SH3 and Ankyrin binding protein 3
mPFC
medial prefrontal cortex
KO
knockout
Het
heterozygote
WT
wild-type
PSD
postsynaptic density
HD
head diameter
PFA
paraformaldehyde
PB
phosphate buffer
ANOVA
analysis of variance
GKAP
guanylate kinase- associated protein
mGluR
metabotropic glutamate receptor
ANK
Ankyrin repeats domain
SH3
SRC homology domain 3
PDZ
PSD-95/Disc Large homolog-1/Zonula occludens-1 domain
PRC
proline-rich cluster domain
SAM
sterile alpha-motif domain
NMDA
N-methyl-D-aspartate

AMPA
amino-3-hydroxy-5-methylisoxazole-4-propionic acid

Declarations

Ethics approval and consent to participate: All animal studies were reviewed and approved by Institutional Animal Care and Use Committee at the Icahn School of Medicine at Mount Sinai.

Consent for publication: Not applicable.

Availability of data and materials: The datasets analyzed during this study are available from the corresponding author on reasonable request.

Competing interests: The authors declare that they have no competing interests.

Funding: This study was supported by funding from Seaver Foundation (to JDB and PRH), the Simons Foundation (Grant 345922 to PRH), the Foundation for Prader–Willi Research (to PRH and MV) and the National Institutes of Health (Grants MH093725 and MH101584 to JDB and PRH).

Authors' contributions: SJ-D performed the analysis of EM images and wrote the initial draft of the paper. NUK acquired the EM images. DLD, BW and WGJ prepared the materials for EM and assisted with manuscript preparation. LH provided critical revisions and scientific input during preparation of the manuscript. HHN and JB provided the animal model and revised the manuscript. MV and PRH oversaw all aspects of experiment design, data analysis and writing the manuscript. MV, PRH, JDB, and HHN designed the study. All authors read and approved the final manuscript. The opinions expressed herein are those of the authors and are not necessarily representative of those of the Uniformed Services University of the Health Sciences, the Department of Defense; or, the United States Army, Navy, or Air Force (DLD).

Acknowledgements: Not applicable.

Authors' information: Not applicable.

References

1. Baio J, Wiggins L, Christensen DL, Maenner MJ, Daniels J, Warren Z, et al. Prevalence of Autism Spectrum Disorder Among Children Aged 8 Years - Autism and Developmental Disabilities Monitoring Network, 11 Sites, United States, 2014. MMWR Surveill Summ. 2018;67(6):1-23.
2. American Psychiatric Association. Diagnostic and statistical Manual of Mental disorders (5th ed.). Washington, DC: American Psychiatric Publishing; 2013.
3. Fernandez BA, Scherer SW. Syndromic autism spectrum disorders: moving from a clinically defined to a molecularly defined approach. Dialogues Clin Neurosci. 2017;19(4):353-71.

4. Ramaswami G, Geschwind DH. Genetics of autism spectrum disorder. Handb Clin Neurol. 2018;147:321-9.
5. Wong AC, Ning Y, Flint J, Clark K, Dumanski JP, Ledbetter DH, et al. Molecular characterization of a 130-kb terminal microdeletion at 22q in a child with mild mental retardation. Am J Hum Genet. 1997;60(1):113-20.
6. Phelan MC, Rogers RC, Saul RA, Stapleton GA, Sweet K, McDermid H, et al. 22q13 deletion syndrome. Am J Med Genet. 2001;101(2):91-9.
7. Soorya L, Kolevzon A, Zweifach J, Lim T, Dobry Y, Schwartz L, et al. Prospective investigation of autism and genotype-phenotype correlations in 22q13 deletion syndrome and SHANK3 deficiency. Mol Autism. 2013;4(1):18.
8. Leblond CS, Nava C, Polge A, Gauthier J, Huguet G, Lumbroso S, et al. Meta-analysis of SHANK Mutations in Autism Spectrum Disorders: a gradient of severity in cognitive impairments. PLoS Genet. 2014;10(9):e1004580.
9. De Rubeis S, Siper PM, Durkin A, Weissman J, Muratet F, Halpern D, et al. Delineation of the genetic and clinical spectrum of Phelan-McDermid syndrome caused by SHANK3 point mutations. Mol Autism. 2018;9:31.
10. Bonaglia MC, Giorda R, Borgatti R, Felisari G, Gagliardi C, Selicorni A, et al. Disruption of the ProSAP2 gene in a t(12;22)(q24.1;q13.3) is associated with the 22q13.3 deletion syndrome. Am J Hum Genet. 2001;69(2):261-8.
11. Wilson HL, Wong AC, Shaw SR, Tse WY, Stapleton GA, Phelan MC, et al. Molecular characterisation of the 22q13 deletion syndrome supports the role of haploinsufficiency of SHANK3/PROSAP2 in the major neurological symptoms. J Med Genet. 2003;40(8):575-84.
12. Luciani JJ, de Mas P, Depetris D, Mignon-Ravix C, Bottani A, Prieur M, et al. Telomeric 22q13 deletions resulting from rings, simple deletions, and translocations: cytogenetic, molecular, and clinical analyses of 32 new observations. J Med Genet. 2003;40(9):690-6.
13. Zwanenburg RJ, Ruiter SA, van den Heuvel ER, Flapper BC, Van Ravenswaaij-Arts CM. Developmental phenotype in Phelan-McDermid (22q13.3 deletion) syndrome: a systematic and prospective study in 34 children. J Neurodev Disord. 2016;8:16.
14. Denayer A, Van Esch H, de Ravel T, Frijns JP, Van Buggenhout G, Vogels A, et al. Neuropsychopathology in 7 Patients with the 22q13 Deletion Syndrome: Presence of Bipolar Disorder and Progressive Loss of Skills. Mol Syndromol. 2012;3(1):14-20.
15. Verhoeven WM, Egger JI, Willemsen MH, de Leijer GJ, Kleefstra T. Phelan-McDermid syndrome in two adult brothers: atypical bipolar disorder as its psychopathological phenotype? Neuropsychiatr Dis Treat. 2012;8:175-9.
16. Vucurovic K, Landais E, Delahaigue C, Eutrope J, Schneider A, Leroy C, et al. Bipolar affective disorder and early dementia onset in a male patient with SHANK3 deletion. Eur J Med Genet. 2012;55(11):625-9.

17. Durand CM, Betancur C, Boeckers TM, Bockmann J, Chaste P, Fauchereau F, et al. Mutations in the gene encoding the synaptic scaffolding protein SHANK3 are associated with autism spectrum disorders. Nat Genet. 2007;39(1):25-7.
18. Moessner R, Marshall CR, Sutcliffe JS, Skaug J, Pinto D, Vincent J, et al. Contribution of SHANK3 mutations to autism spectrum disorder. Am J Hum Genet. 2007;81(6):1289-97.
19. Sheng M, Kim E. The Shank family of scaffold proteins. J Cell Sci. 2000;113 (Pt 11):1851-6.
20. Naisbitt S, Kim E, Tu JC, Xiao B, Sala C, Valtschanoff J, et al. Shank, a novel family of postsynaptic density proteins that binds to the NMDA receptor/PSD-95/GKAP complex and cortactin. Neuron. 1999;23(3):569-82.
21. Lim S, Naisbitt S, Yoon J, Hwang JI, Suh PG, Sheng M, et al. Characterization of the Shank family of synaptic proteins. Multiple genes, alternative splicing, and differential expression in brain and development. J Biol Chem. 1999;274(41):29510-8.
22. Boeckers TM, Winter C, Smalla KH, Kreutz MR, Bockmann J, Seidenbecher C, et al. Proline-rich synapse-associated proteins ProSAP1 and ProSAP2 interact with synaptic proteins of the SAPAP/GKAP family. Biochem Biophys Res Commun. 1999;264(1):247-52.
23. Sala C, Vicidomini C, Bigi I, Mossa A, Verpelli C. Shank synaptic scaffold proteins: keys to understanding the pathogenesis of autism and other synaptic disorders. J Neurochem. 2015;135(5):849-58.
24. Tu JC, Xiao B, Naisbitt S, Yuan JP, Petralia RS, Brakeman P, et al. Coupling of mGluR/Homer and PSD-95 complexes by the Shank family of postsynaptic density proteins. Neuron. 1999;23(3):583-92.
25. Jiang YH, Ehlers MD. Modeling autism by SHANK gene mutations in mice. Neuron. 2013;78(1):8-27.
26. Uchino S, Wada H, Honda S, Nakamura Y, Ondo Y, Uchiyama T, et al. Direct interaction of post-synaptic density-95/Dlg/ZO-1 domain-containing synaptic molecule Shank3 with GluR1 alpha-amino-3-hydroxy-5-methyl-4-isoxazole propionic acid receptor. J Neurochem. 2006;97(4):1203-14.
27. Du Y, Weed SA, Xiong WC, Marshall TD, Parsons JT. Identification of a novel cortactin SH3 domain-binding protein and its localization to growth cones of cultured neurons. Mol Cell Biol. 1998;18(10):5838-51.
28. Boeckers TM, Liedtke T, Spilker C, Dresbach T, Bockmann J, Kreutz MR, et al. C-terminal synaptic targeting elements for postsynaptic density proteins ProSAP1/Shank2 and ProSAP2/Shank3. J Neurochem. 2005;92(3):519-24.
29. Tao-Cheng JH, Dosemeci A, Gallant PE, Smith C, Reese T. Activity induced changes in the distribution of Shanks at hippocampal synapses. Neuroscience. 2010;168(1):11-7.
30. Fuster JM. The prefrontal cortex--an update: time is of the essence. Neuron. 2001;30(2):319-33.
31. Miller EK, Cohen JD. An integrative theory of prefrontal cortex function. Annu Rev Neurosci. 2001;24:167-202.
32. Liakakis G, Nickel J, Seitz RJ. Diversity of the inferior frontal gyrus--a meta-analysis of neuroimaging studies. Behav Brain Res. 2011;225(1):341-7.

33. Ariza J, Rogers H, Hashemi E, Noctor SC, Martinez-Cerdeno V. The Number of Chandelier and Basket Cells Are Differentially Decreased in Prefrontal Cortex in Autism. Cereb Cortex. 2018;28(2):411-20.
34. Courchesne E, Mouton PR, Calhoun ME, Semendeferi K, Ahrens-Barbeau C, Hallet MJ, et al. Neuron number and size in prefrontal cortex of children with autism. JAMA. 2011;306(18):2001-10.
35. Hashemi E, Ariza J, Rogers H, Noctor SC, Martinez-Cerdeno V. The Number of Parvalbumin-Expressing Interneurons Is Decreased in the Prefrontal Cortex in Autism. Cereb Cortex. 2018;28(2):690.
36. Jacot-Descombes S, Uppal N, Wicinski B, Santos M, Schmeidler J, Giannakopoulos P, et al. Decreased pyramidal neuron size in Brodmann areas 44 and 45 in patients with autism. Acta Neuropathol. 2012;124(1):67-79.
37. Hazlett HC, Poe MD, Gerig G, Styner M, Chappell C, Smith RG, et al. Early brain overgrowth in autism associated with an increase in cortical surface area before age 2 years. Arch Gen Psychiatry. 2011;68(5):467-76.
38. Schumann CM, Bloss CS, Barnes CC, Wideman GM, Carper RA, Akshoomoff N, et al. Longitudinal magnetic resonance imaging study of cortical development through early childhood in autism. J Neurosci. 2010;30(12):4419-27.
39. McGaughy J, Ross RS, Eichenbaum H. Noradrenergic, but not cholinergic, deafferentation of prefrontal cortex impairs attentional set-shifting. Neuroscience. 2008;153(1):63-71.
40. Pezze M, McGarrity S, Mason R, Fone KC, Bast T. Too little and too much: hypoactivation and disinhibition of medial prefrontal cortex cause attentional deficits. J Neurosci. 2014;34(23):7931-46.
41. Park J, Moghaddam B. Impact of anxiety on prefrontal cortex encoding of cognitive flexibility. Neuroscience. 2017;345:193-202.
42. Wang J, Qu S, Wang W, Guo L, Zhang K, Chang S, et al. A combined analysis of genome-wide expression profiling of bipolar disorder in human prefrontal cortex. J Psychiatr Res. 2016;82:23-9.
43. Selemon LD, Zecevic N. Schizophrenia: a tale of two critical periods for prefrontal cortical development. Transl Psychiatry. 2015;5:e623.
44. Zhou Y, Fan L, Qiu C, Jiang T. Prefrontal cortex and the dysconnectivity hypothesis of schizophrenia. Neurosci Bull. 2015;31(2):207-19.
45. Lord C, Elsabbagh M, Baird G, Veenstra-Vanderweele J. Autism spectrum disorder. Lancet. 2018;392(10146):508-20.
46. Aldinger KA, Lane CJ, Veenstra-VanderWeele J, Levitt P. Patterns of Risk for Multiple Co-Occurring Medical Conditions Replicate Across Distinct Cohorts of Children with Autism Spectrum Disorder. Autism Res. 2015;8(6):771-81.
47. Laubach M, Amarante LM, Swanson K, White SR. What, If Anything, Is Rodent Prefrontal Cortex? eNeuro. 2018;5(5).
48. Laroche S, Davis S, Jay TM. Plasticity at hippocampal to prefrontal cortex synapses: dual roles in working memory and consolidation. Hippocampus. 2000;10(4):438-46.

49. Heidbreder CA, Groenewegen HJ. The medial prefrontal cortex in the rat: evidence for a dorso-ventral distinction based upon functional and anatomical characteristics. Neurosci Biobehav Rev. 2003;27(6):555-79.
50. Quirk GJ, Beer JS. Prefrontal involvement in the regulation of emotion: convergence of rat and human studies. Curr Opin Neurobiol. 2006;16(6):723-7.
51. Vertes RP. Interactions among the medial prefrontal cortex, hippocampus and midline thalamus in emotional and cognitive processing in the rat. Neuroscience. 2006;142(1):1-20.
52. Kesner RP, Churchwell JC. An analysis of rat prefrontal cortex in mediating executive function. Neurobiol Learn Mem. 2011;96(3):417-31.
53. Roussignol G, Ango F, Romorini S, Tu JC, Sala C, Worley PF, et al. Shank expression is sufficient to induce functional dendritic spine synapses in aspiny neurons. J Neurosci. 2005;25(14):3560-70.
54. Baron MK, Boeckers TM, Vaida B, Faham S, Gingery M, Sawaya MR, et al. An architectural framework that may lie at the core of the postsynaptic density. Science. 2006;311(5760):531-5.
55. Harony-Nicolas H, Kay M, du Hoffmann J, Klein ME, Bozdagi-Gunal O, Riad M, et al. Oxytocin improves behavioral and electrophysiological deficits in a novel Shank3-deficient rat. Elife. 2017;6.
56. Hamdan FF, Gauthier J, Araki Y, Lin DT, Yoshizawa Y, Higashi K, et al. Excess of de novo deleterious mutations in genes associated with glutamatergic systems in nonsyndromic intellectual disability. Am J Hum Genet. 2011;88(3):306-16.
57. Bloss EB, Puri R, Yuk F, Punsoni M, Hara Y, Janssen WG, et al. Morphological and molecular changes in aging rat prelimbic prefrontal cortical synapses. Neurobiol Aging. 2013;34(1):200-10.
58. Sterio DC. The unbiased estimation of number and sizes of arbitrary particles using the disector. J Microsc. 1984;134(Pt 2):127-36.
59. Uppal N, Puri R, Yuk F, Janssen WG, Bozdagi-Gunal O, Harony-Nicolas H, et al. Ultrastructural analyses in the hippocampus CA1 field in Shank3-deficient mice. Mol Autism. 2015;6:41.
60. Ziats CA, Grosvenor LP, Sarasua SM, Thurm AE, Swedo SE, Mahfouz A, et al. Functional genomics analysis of Phelan-McDermid syndrome 22q13 region during human neurodevelopment. PLoS One. 2019;14(3):e0213921.
61. Waga C, Asano H, Sanagi T, Suzuki E, Nakamura Y, Tsuchiya A, et al. Identification of two novel Shank3 transcripts in the developing mouse neocortex. J Neurochem. 2014;128(2):280-93.
62. Wang X, Xu Q, Bey AL, Lee Y, Jiang YH. Transcriptional and functional complexity of Shank3 provides a molecular framework to understand the phenotypic heterogeneity of SHANK3 causing autism and Shank3 mutant mice. Mol Autism. 2014;5:30.
63. Ching TT, Maunakea AK, Jun P, Hong C, Zardo G, Pinkel D, et al. Epigenome analyses using BAC microarrays identify evolutionary conservation of tissue-specific methylation of SHANK3. Nat Genet. 2005;37(6):645-51.
64. Maunakea AK, Nagarajan RP, Bilenky M, Ballinger TJ, D'Souza C, Fouse SD, et al. Conserved role of intragenic DNA methylation in regulating alternative promoters. Nature. 2010;466(7303):253-7.

65. Zhu L, Wang X, Li XL, Towers A, Cao X, Wang P, et al. Epigenetic dysregulation of SHANK3 in brain tissues from individuals with autism spectrum disorders. Hum Mol Genet. 2014;23(6):1563-78.
66. Ehlers MD. Activity level controls postsynaptic composition and signaling via the ubiquitin-proteasome system. Nat Neurosci. 2003;6(3):231-42.
67. Duffney LJ, Zhong P, Wei J, Matas E, Cheng J, Qin L, et al. Autism-like Deficits in Shank3-Deficient Mice Are Rescued by Targeting Actin Regulators. Cell Rep. 2015;11(9):1400-13.
68. Kouser M, Speed HE, Dewey CM, Reimers JM, Widman AJ, Gupta N, et al. Loss of predominant Shank3 isoforms results in hippocampus-dependent impairments in behavior and synaptic transmission. J Neurosci. 2013;33(47):18448-68.
69. Gouder L, Vitrac A, Goubran-Botros H, Danckaert A, Tinevez JY, Andre-Leroux G, et al. Altered spinogenesis in iPSC-derived cortical neurons from patients with autism carrying de novo SHANK3 mutations. Sci Rep. 2019;9(1):94.
70. Zhao H, Tu Z, Xu H, Yan S, Yan H, Zheng Y, et al. Altered neurogenesis and disrupted expression of synaptic proteins in prefrontal cortex of SHANK3-deficient non-human primate. Cell Res. 2017;27(10):1293-7.
71. Song TJ, Lan XY, Wei MP, Zhai FJ, Boeckers TM, Wang JN, et al. Altered Behaviors and Impaired Synaptic Function in a Novel Rat Model With a Complete Shank3 Deletion. Front Cell Neurosci. 2019;13:111.
72. Peca J, Feliciano C, Ting JT, Wang W, Wells MF, Venkatraman TN, et al. Shank3 mutant mice display autistic-like behaviours and striatal dysfunction. Nature. 2011;472(7344):437-42.
73. Kloth AD, Badura A, Li A, Cherskov A, Connolly SG, Giovannucci A, et al. Cerebellar associative sensory learning defects in five mouse autism models. Elife. 2015;4:e06085.
74. Wang X, McCoy PA, Rodriguiz RM, Pan Y, Je HS, Roberts AC, et al. Synaptic dysfunction and abnormal behaviors in mice lacking major isoforms of Shank3. Hum Mol Genet. 2011;20(15):3093-108.
75. Wang X, Bey AL, Katz BM, Badea A, Kim N, David LK, et al. Altered mGluR5-Homer scaffolds and corticostriatal connectivity in a Shank3 complete knockout model of autism. Nat Commun. 2016;7:11459.
76. Jones DG, Harris RJ. An analysis of contemporary morphological concepts of synaptic remodelling in the CNS: perforated synapses revisited. Rev Neurosci. 1995;6(3):177-219.
77. Geinisman Y, Disterhoft JF, Gundersen HJ, McEchron MD, Persina IS, Power JM, et al. Remodeling of hippocampal synapses after hippocampus-dependent associative learning. J Comp Neurol. 2000;417(1):49-59.
78. Geinisman Y, de Toledo-Morrell L, Morrell F. Loss of perforated synapses in the dentate gyrus: morphological substrate of memory deficit in aged rats. Proc Natl Acad Sci U S A. 1986;83(9):3027-31.
79. Geinisman Y, de Toledo-Morrell L, Morrell F. Aged rats need a preserved complement of perforated axospinous synapses per hippocampal neuron to maintain good spatial memory. Brain Res.

1986;398(2):266-75.
80. MacGillavry HD, Kerr JM, Kassner J, Frost NA, Blanpied TA. Shank-cortactin interactions control actin dynamics to maintain flexibility of neuronal spines and synapses. Eur J Neurosci. 2016;43(2):179-93.
81. Sala C, Piech V, Wilson NR, Passafaro M, Liu G, Sheng M. Regulation of dendritic spine morphology and synaptic function by Shank and Homer. Neuron. 2001;31(1):115-30.
82. Verpelli C, Dvoretskova E, Vicidomini C, Rossi F, Chiappalone M, Schoen M, et al. Importance of Shank3 protein in regulating metabotropic glutamate receptor 5 (mGluR5) expression and signaling at synapses. J Biol Chem. 2011;286(40):34839-50.
83. Lee Y, Kang H, Lee B, Zhang Y, Kim Y, Kim S, et al. Integrative Analysis of Brain Region-specific Shank3 Interactomes for Understanding the Heterogeneity of Neuronal Pathophysiology Related to SHANK3 Mutations. Front Mol Neurosci. 2017;10:110.
84. Wang ZJ, Zhong P, Ma K, Seo JS, Yang F, Hu Z, et al. Amelioration of autism-like social deficits by targeting histone methyltransferases EHMT1/2 in Shank3-deficient mice. Mol Psychiatry. 2019.
85. Ma K, Qin L, Matas E, Duffney LJ, Liu A, Yan Z. Histone deacetylase inhibitor MS-275 restores social and synaptic function in a Shank3-deficient mouse model of autism. Neuropsychopharmacology. 2018;43(8):1779-88.
86. Lee J, Chung C, Ha S, Lee D, Kim DY, Kim H, et al. Shank3-mutant mice lacking exon 9 show altered excitation/inhibition balance, enhanced rearing, and spatial memory deficit. Front Cell Neurosci. 2015;9:94.
87. Romorini S, Piccoli G, Jiang M, Grossano P, Tonna N, Passafaro M, et al. A functional role of postsynaptic density-95-guanylate kinase-associated protein complex in regulating Shank assembly and stability to synapses. J Neurosci. 2004;24(42):9391-404.
88. Im YJ, Lee JH, Park SH, Park SJ, Rho SH, Kang GB, et al. Crystal structure of the Shank PDZ-ligand complex reveals a class I PDZ interaction and a novel PDZ-PDZ dimerization. J Biol Chem. 2003;278(48):48099-104.
89. Berg EL, Copping NA, Rivera JK, Pride MC, Careaga M, Bauman MD, et al. Developmental social communication deficits in the Shank3 rat model of phelan-mcdermid syndrome and autism spectrum disorder. Autism Res. 2018;11(4):587-601.
90. Phelan MC. Deletion 22q13.3 syndrome. Orphanet J Rare Dis. 2008;3:14.

Figures

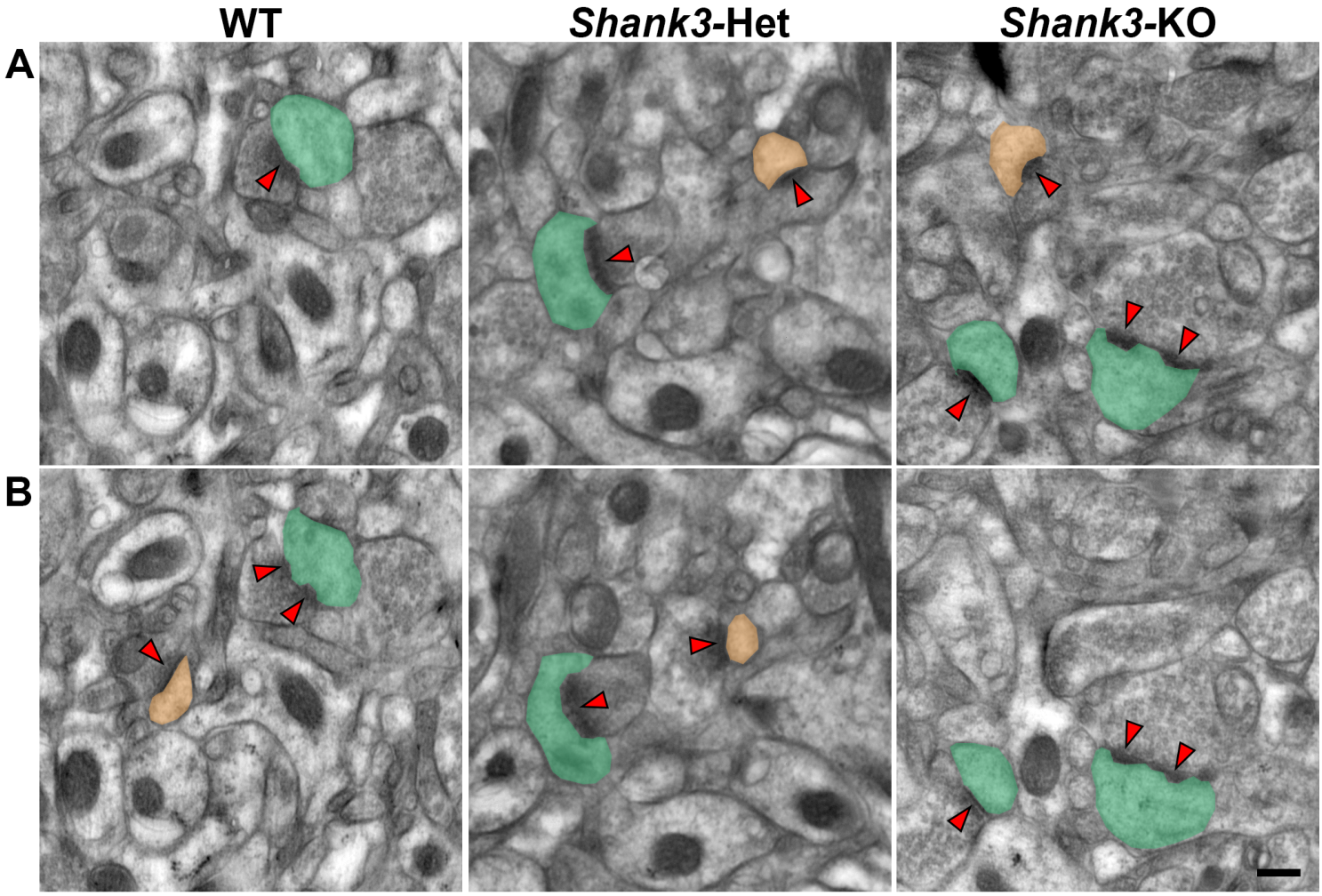

Figure 1

Disector method for estimation of synapse density. Electron micrographs showing examples of (A) reference layers with (B) their associated lookup layers. The orange masks indicate the postsynaptic spine of unique synapses, seen only in the reference layer or the lookup layer. The green masks show the postsynaptic spine of synapses seen in both layers. The red arrowheads indicate electron-dense PSDs. Note the split PSDs in the perforated synapses. Scale bar = 250 nm. WT = wild-type; Shank3-Het = Shank3 heterozygotes; Shank3-KO = Shank3 knockouts.

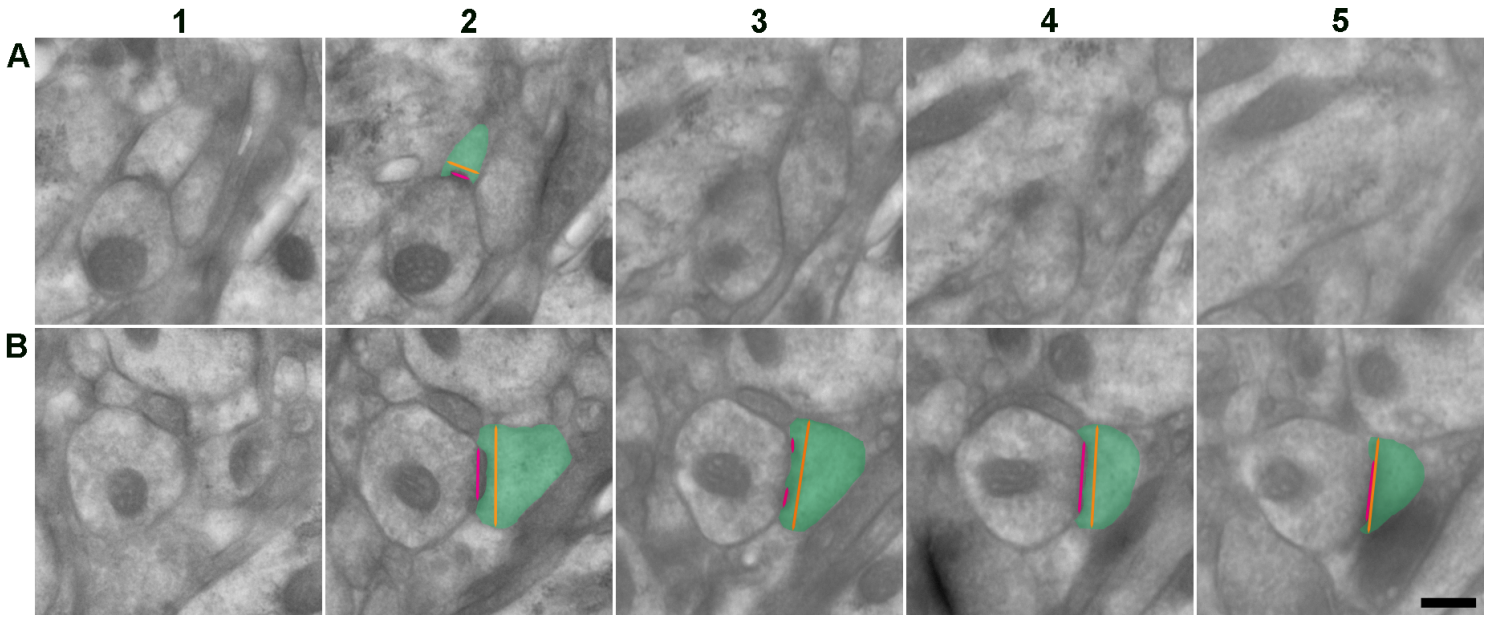

Figure 2

Measurement of PSD length and HD in non-perforated and perforated synapses. Electron micrographs selected from two sets of five serial sections each to depict (A) a unique non-perforated synapse and (B) a perforated synapse. The sections are numbered 1 to 5 to show their position in the series. The postsynaptic spine of unique synapses is indicated in green. PSD length (magenta line) and HD (orange line) were measured for each non-perforated synapse and in all the sections where it was visible for the perforated synapse. Scale bar = 250 nm.

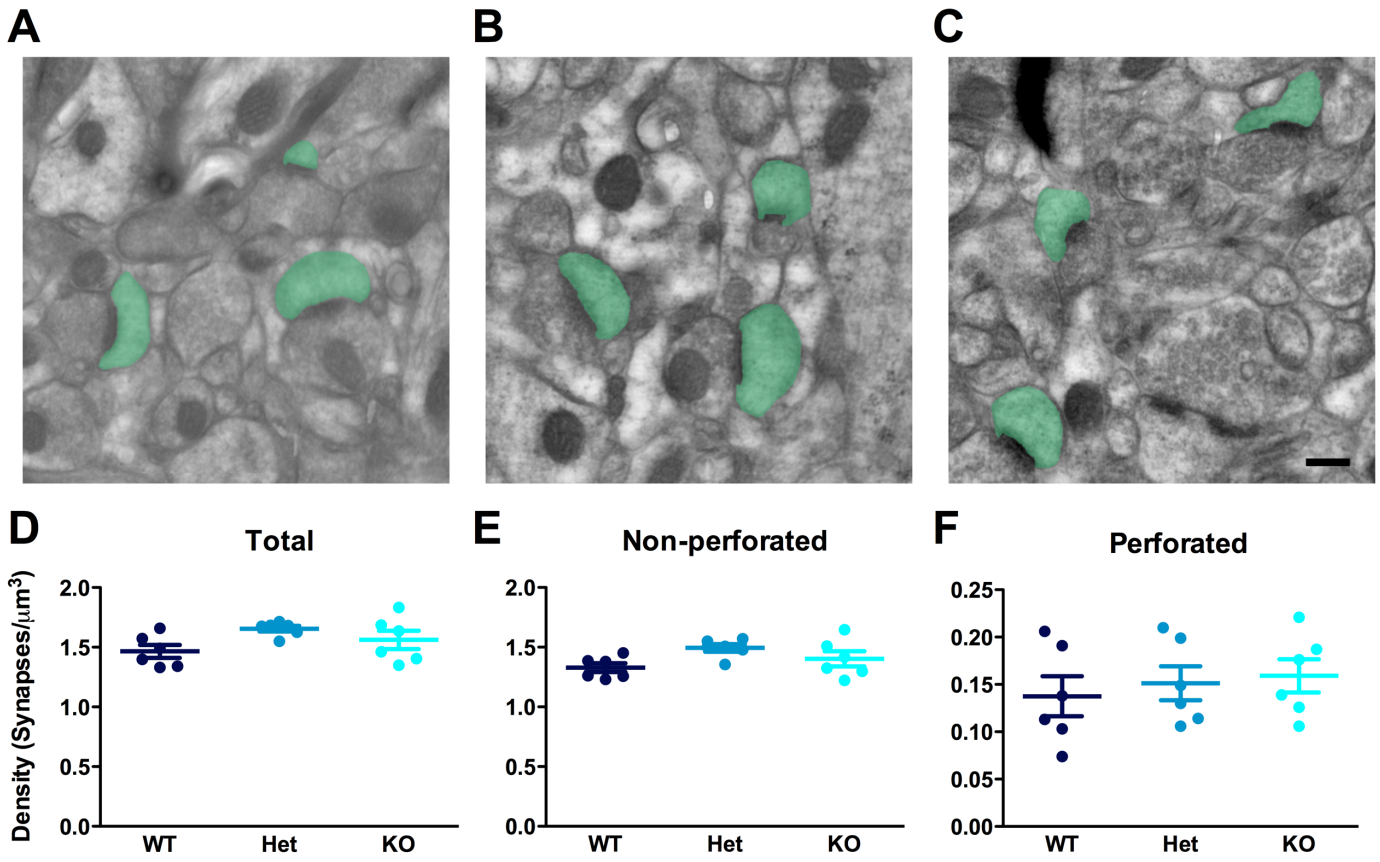

Figure 3

Synapse densities were comparable in WT, Shank3-Het and Shank3-KO rats. Representative sections from (A) WT, (B) Shank3-Het, and (C) Shank3-KO rats showing unique synapses. The postsynaptic spine of unique synapses is indicated in green. Scale bar = 250 nm. (D) Total synapse density, (E) non-perforated synapse density, and (F) perforated synapse density were similar in all three groups. WT = wild-type; Het = Shank3 heterozygotes; KO = Shank3 knockouts.

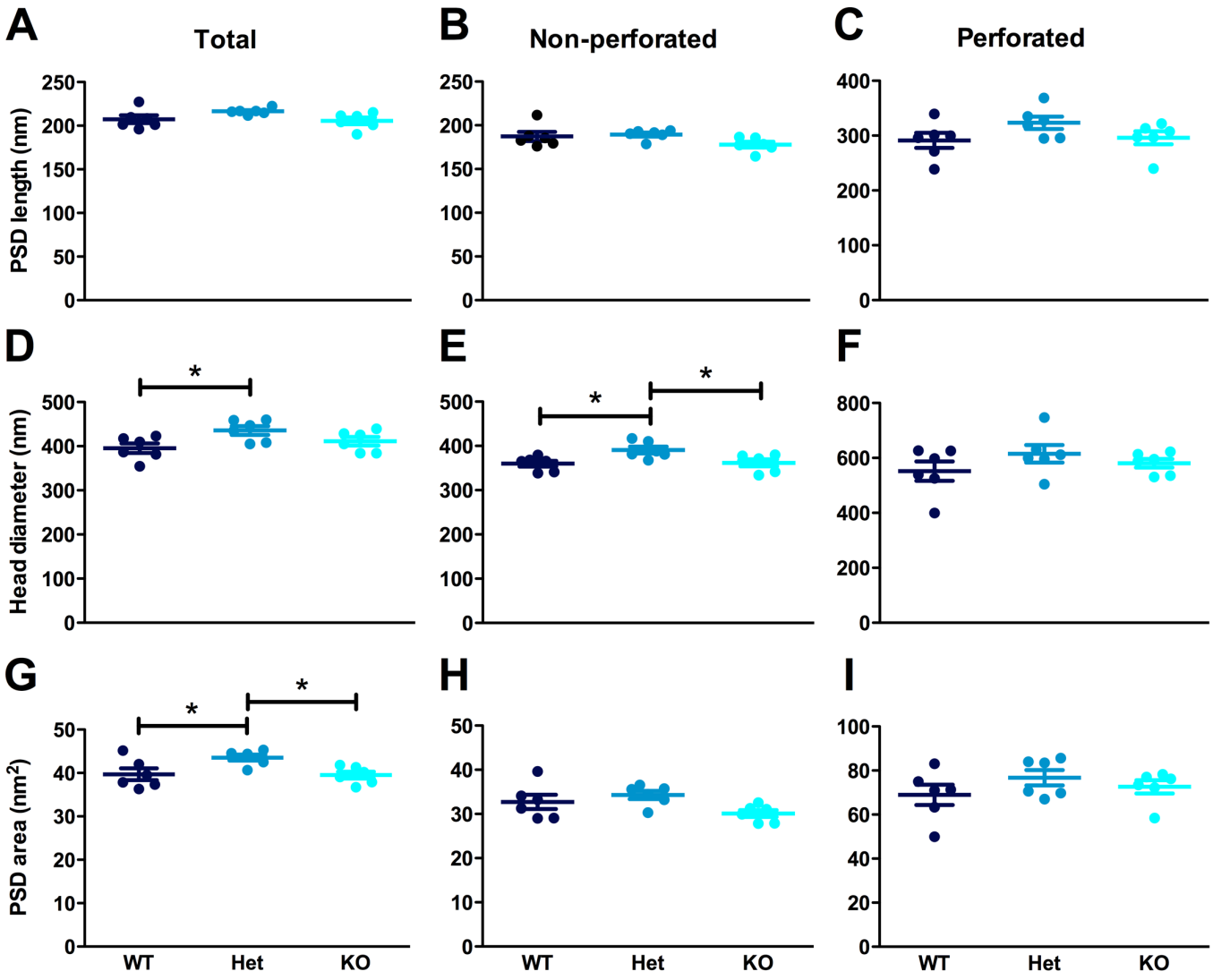

Figure 4

PSD length was comparable, but HD and PSD area were higher in Shank3-Het compared to WT rats. (A-I). PSD length in (A) total synapses, (B) non-perforated synapses, as well (C) perforated synapses are comparable among WT, Shank3-Het, and Shank3-KO rats. (D) HD in total synapses is wider in Shank3-Het rats compared to the WT. (E) HD in non-perforated synapses is wider in Shank3-Het rats compared to both WT and Shank3-KO, but non-perforated synapses in the Shank3-KO have similar HD as the WT. (F) HD of perforated synapses are comparable in WT, Shank3-Het and Shank3-KO. (G) The Shank3-Het group has greater PSD area of total synapses compared to the WT and Shank3-KO, but the Shank3-KO and WT are comparable for this measure. PSD area of (H) non-perforated and (I) perforated synapses are similar among the three groups. WT = wild-type; Het = Shank3 heterozygotes; KO = Shank3 knockouts. * indicates $p < 0.05$ by one-way ANOVA followed by Tukey's test as compared to the indicated group.